Т. 88, № 3 **ЖУРНАЛ ПРИКЛАДНОЙ СПЕКТРОСКОПИИ** МАЙ — ИЮНЬ 2021

V. 88, N 3 **JOURNAL OF APPLIED SPECTROSCOPY** MAY — JUNE 2021

INFRARED LINE COLLISIONAL PARAMETERS OF PH_3 IN HYDROGEN: MEASUREMENTS WITH SECOND-ORDER APPROXIMATION OF PERTURBATION THEORY

J. Salem [1], R. Charguia [2,3*], R. ben Younes [1]

[1] Laboratoire Technologie Energie et Matériaux Innovants TEMI, Faculté des Sciences de Gafsa,
Campus Universitaire Sidi Ahmed Zarroug -2112 Gafsa, Tunisia
[2] Department of Physics, College of Sciences and Arts at Buraydah, Qassim University, Saudi Arabia;
e-mail: charguiaraihen@yahoo.fr
[3] Condensed Matter Physics Laboratory, Physics Department, Faculty of Sciences of Tunis,
University of Tunis El Manar, 1060 Tunis, Tunisia

Room-temperature absorption by PH_3–H_2 mixtures in the ν_2 and ν_4 bands of phosphine (PH_3) has been measured for low pressures. Fits of these spectra are made to determine the width of isolated lines and line mixing in a first-order Rosenkranz approximation. From the previous determinations, we deduce remarks on the lack of accuracy of predicting the collisional process. With the first-order Rosenkranz approximation, the collisional parameters are considered linear with pressure. In this work, we have considered spectra recorded for three doublets: A_1 and A_2 lines in the ν_2 and ν_4 bands of PH_3 diluted with higher H_2 pressure. We show that the line shifts are non-linear with perturber pressures, which requires testing the fits of the recorded spectra with profiles developed in the second-order approximation of the perturbation theory. Consequently, the first- and second-order mixing coefficients are determined and discussed. Throughout this study, we also show that the change in the intensity distribution is provided by the population exchange between low energy levels for the two components of doublets A_1 and A_2 lines and is described through the second-order mixing parameter. Thereby, we show the mixing effect on line width.

Keywords: *first-order Rosenkranz approximation, second-order approximation, perturbation theory.*

ИЗМЕРЕНИЯ И РАСЧЕТ ВО ВТОРОМ ПОРЯДКЕ ТЕОРИИ ВОЗМУЩЕНИЙ СТОЛКНОВИТЕЛЬНЫХ ПАРАМЕТРОВ ИК-ЛИНИЙ PH_3 В ВОДОРОДЕ

J. Salem [1], R. Charguia [2,3*], R. ben Younes [1]

УДК 535.34:546.11

[1] Университет Сиди Ахмед Зарруга, 2112 Гафса, Тунис
[2] Колледж наук и искусств Бурайды Университета Кассима,
Саудовская Аравия; e-mail: charguiaraihen@yahoo.fr
[3] Тунисский университет Эль-Манар, 1060 Тунис, Тунис

(Поступила 13 апреля 2020)

Поглощение при комнатной температуре смесями PH_3–H_2 в полосах ν_2 и ν_4 фосфина (PH_3) измерено для низких давлений. Подбор спектров выполняется для определения ширины изолированных линий и смешивания линий в приближении Розенкранца первого порядка. В приближении Розенкранца первого порядка параметры столкновения считаются линейными с давлением. Зарегистрированы спектры для трех дублетов: линии A_1 и A_2 в полосах ν_2 и ν_4 PH_3, разбавленного H_2 более высокого давления. Показано, что сдвиги линий не линейны в зависимости от возмущающего давления. Это требует проверки соответствия записанных спектров профилям, полученным во втором порядке теории возмущений. Определяются и обсуждаются коэффициенты смешивания первого и второго *порядка. Показано, что изменение распределения интенсивности обеспечивается обменом населенностью между низкими энергетическими уровнями для компонентов дублетов A_1 и A_2 и описывается с помощью параметра смешения второго порядка. Таким образом смешивание влияет на ширину линии.*

Ключевые слова: *приближение Розенкранца первого порядка, приближение второго порядка, теория возмущений.*

Introduction. Phosphine is a molecule observed in the atmosphere of Jupiter and Saturn [1–4] and is composed mainly of hydrogen and helium. In addition, the study of its broadened spectra by H_2 pressure can be useful in modeling planetary atmospheres. Therefore, it is of astrophysical interest. Moreover, the study of their overlapping lines can provide information on the collisional dynamics of this molecule as well as on the radiative transfer between relative transitions, which are of fundamental interest.

To model a rovibrational spectrum, different procedures and approximations have been established to adjust the spectral lines of some molecules in the infrared (IR) region. In the framework of isolated line approximation, the absorption lines of the ν_2 and ν_4 bands of phosphine (PH_3), recorded using a diode-laser spectrometer, are fitted with the Voigt, Rautian, and speed-dependent Rautian profiles [5–10]. In the framework of a first-order Rosenkranz approximation, some experimental spectra of the same ν_2 and ν_4 bands of PH_3 diluted with hydrogen (H_2) at room and low temperatures were analyzed with non-linear least-squares multi-pressure fitting procedures based on the collisional Rosenkranz profile [11, 12]. In other works, the rovibrational spectra of other molecules, such as CH_4, NH_3, CH_3Br, and C_3H_4, are fitted using the same procedures [13–16].

The collisional line width shows a linear regression with the perturber pressure. The same applies to the intensity parameter vs. the pressure of the active gas. Conversely, in some papers, the line shift shows a nonlinear variation with perturber pressure [14, 17, 18], which is inconsistent with the hypotheses of isolated lines and first-order Rosenkranz approximations. In fact, the reconstruction of collisional profiles is based on the diagonalization of the relaxation matrix as part of the impact approximation. A simple and well-known method of calculation is the perturbation theory used in the construction of the profiles previously mentioned. Smith [19] extended the first-order Rosenkranz approximation [20] to the second order in the framework of perturbation theory. His work yields a collisional profile, considering the first- and second-order parameters of line mixing effects. In this same profile expression, the line shift vs. the perturber pressure has a parabolic form.

We have used the collisional profile expression given by Smith to analyze some spectra of three doublets A_1 and A_2 line recorded using a diode-laser spectrometer in the ν_2 and ν_4 bands of PH_3 diluted with H_2 at higher pressure and room temperature. Then, we specified the collisional parameters to adjust. In addition, the reconstruction of the recorded spectra justifies the need to consider second-order mixing and shifting parameters. Consequently, the first- and second-order H_2-line mixing coefficients in the ν_2 and ν_4 bands of PH_3 are presented and discussed. Through this study, we show the line mixing effect on the intensity distributions and line widths.

Experimental analysis. *Experimental conditions.* The absorption spectra of the PH_3-H_2 mixture in the ν_2 and ν_4 bands of phosphine were recorded at high resolution using a tunable diode-laser spectrometer (Laser Analytics Model LS3). The experimental techniques are detailed in [21, 22]. In this work, we give the experimental conditions of the measurements, verifying our analytic procedure.

The absorption path length of the IR radiation provided by the diode laser in the multipass white-type cell is fixed to 20.17 m. The phosphine sample is supplied by Union Carbide with a stated purity of 99.999%, and the hydrogen sample is supplied by Air Liquide with a stated purity of 99.99%. The gas pressure is measured by two Baratron MKS gauges with full-scale measurements of 1.2 and 120 mbar, with an accuracy of 5×10^{-4} and 2×10^{-2} mbar. All spectra are recorded at room temperature (297.2±1.5 K). Table 1 summarizes the data needed for the transitions studied in this work: wave numbers, pressure of PH_3 (P_{PH3}), Doppler half-width (γ_{Dop}), effective Doppler half-width (γ_{Deff}), temperature T, and pressure of H_2 (P_{H2}). Moreover, Fig. 1 shows an example of the recorded spectra of the doublet ${}^RR(4,3,A_1)$ and ${}^RR(4,3,A_2)$ lines of the ν_4 band of PH_3 diluted with pressures of H_2, where the transmittance is plotted vs. the point numbers. The relative calibration of spectra is performed using a confocal etalon with an inter-fringe spacing of 0.007958 cm^{-1}. The etalon fringe pattern provides a check of the laser mode's quality for correcting the slightly nonlinear tuning of the diode laser. Furthermore, it aids in linearization of the spectra with a constant step of 0.000121 cm^{-1}. All spectra are linearized using the cubic splines techniques [23].

TABLE 1. Experimental Conditions of the Recorded Spectra

Transition	σ, cm^{-1} [24]	P_{PH_3}, mbar	γ_{Dop}, 10^{-3} cm^{-1}	γ_{Deff}, 10^{-3} cm^{-1}	T, K	P_{H_2}, mbar
ν_2 band						
$^QR(8,3,A_1)$	1059.14042	0.0010	1.1248	1.1484	298.15	55.14, 65.88, 80.70, 102.29
$^QR(8,3,A_2)$	1059.14988			1.1473		P_{PH_3} = 0.022 mbar
$^QR(9,3,A_1)$	1065.05928	0.0009	1.1299	1.2220	297.65	59.13, 72.86, 86.15, 111.20
$^QR(9,3,A_2)$	1065.07558			1.2039		P_{PH_3} = 0.021 mbar
ν_4 band						
$^RR(4,3,A_1)$	1174.62613	0.0009	1.2466	1.3454	297.75	70.71, 82.86, 100.77, 116.80
$^RR(4,3,A_2)$	1174.64546			1.3464		P_{PH_3} = 0.029 mbar

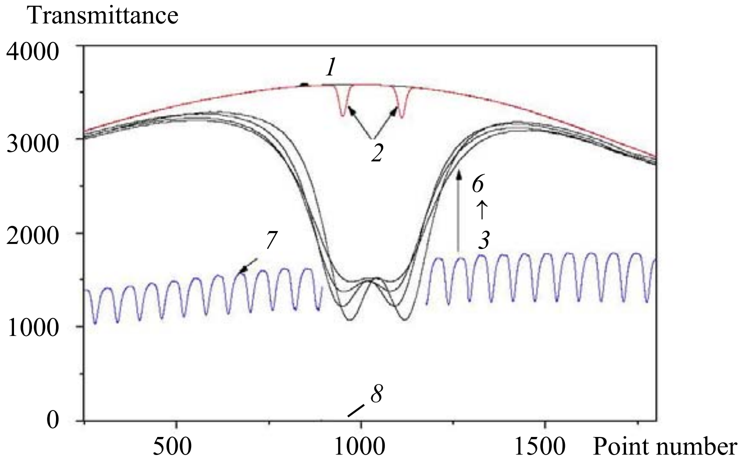

Fig. 1. Recorded spectra for the A_1A_2 components of the $^RR(4,3)$ doublet transition in the ν_4 band of PH_3 diluted by H_2. 1) Baseline recorded with an empty cell; 2) effective Doppler lines recorded at a low pressure of pure PH_3 0.029 mbar; 3–6) records of the broadened at pressures of H_2 70.71, 82.86, 100.77, and 116.80 mbar, respectively; 7) confocal etalon fringes pattern; 8) 0% transmission level.

Profiles and fitting procedure. The spectra recorded using the diode-laser spectrometer allow the writing of the Beer–Lambert law:

$$\alpha(\sigma) = (1/l)\ln[I_0(\sigma)/I_t(\sigma)], \tag{1}$$

where $\alpha(\sigma)$ is the experimental absorbance per unit length at wavenumber σ in cm^{-1}, l is the path length, and $I_0(\sigma)$ and $I_t(\sigma)$ are the transmitted intensities measured with the cell under a vacuum and filled with the gas sample, respectively. To fit the recorded spectra, three physical effects must be considered: weak instrumental distortion and Doppler and collisional effects. The first is implicitly considered through the effective half-width γ_{Deff} obtained by fitting the effective Doppler line [25] (Table 1). The Voigt profile (VP) results from the convolution of the Doppler and collisional profiles, reflecting the latter two effects. The expression of this profile depends on the extension of the collisional profile to be considered.

Consider the collisional profile proposed by Smith [19] and developed within the framework of the second-order approximation of perturbation theory:

$$\alpha_C(\sigma) = \frac{P_{PH_3}}{\pi}\sum_{\text{line}\,k} S_k\left[\frac{\gamma_k(1+P^2g_k)+(\sigma-\sigma_k+P^2\delta\sigma_k)PY_k}{(\sigma-\sigma_k+P^2\delta\sigma_k)^2+\gamma_k{}^2}\right], \tag{2}$$

where the index k represents transitions in Liouville or “line” space, and S_k, γ_k, and Y_k are the coupled line strength, the collisional half-width, and the first-order line mixing coefficient, respectively. The wavenumber $\sigma_k = \sigma_{0k} - \delta_k$, where σ_{0k} is the line center wavenumber and δ_k is the line shift. In addition, g_k is the second-order line-mixing coefficient, and $\delta\sigma_k$ is the second-order line-shift coefficient. We deduce the Voigt profile (VPI2) corresponding to this collisional profile as

$$\alpha_{VPI2}(\sigma) = \frac{P_{\mathrm{PH_3}}}{\gamma_{\mathrm{Deff}}\sqrt{\pi}} \sum_{\text{line } k} S_k \left\{\left(1+P^2 g_k\right)\mathrm{Re}\left[W(x,y)\right] + PY_k \,\mathrm{Im}\left[W(x,y)\right]\right\}, \tag{3}$$

where $W(x,y)$ is the complex probability function expressed by [26]:

$$W(x,y) = \left(\frac{i}{\pi}\right)\int_{-\infty}^{+\infty} \frac{e^{-t^2}}{x-t+iy}\,dt, \tag{4}$$

where $x = (\ln 2)^{1/2}(\sigma - \sigma_k + P^2\delta\sigma_k)/\gamma_{\mathrm{Deff}}$ and $y = (\ln 2)^{1/2}\gamma_k/\gamma_{\mathrm{Deff}}$.

It should be noted that the parameters σ_k, $P^2\delta\sigma_k$, γ_k, PY_k, and P^2g_k are related to the diagonal (W_{kk}) and off-diagonal ($W_{kk'}$ with $k' \neq k$) elements of the collisional relaxation matrix (W) [19]. If the second-order parameters ($\delta\sigma_k$ and g_k) equal zero, then Eq. (3) reduces to the expression of the first-order Rosenkranz approximation model (VPI1) [18, 27].

To fit the observed spectra, we set the intensity parameter to the value deduced from the absolute line intensity [18]. Figure 2 shows an example of the fits for the A_1 and A_2 lines of the doublet $^{R}R(4,3)$ in the ν_4 band of PH_3 diluted with 100.77 mbar of H_2 by the theoretical profiles VPI1 and VPI2. The (Obs-Calc) residuals are multiplied by 5 and displaced vertically for visibility. The (Obs-Calc) residuals of VPI2 show a better reproduction of the observed lines than that given by VPI1, where the second-order line mixing parameter is not considered. The better reconstruction given by VPI2 mainly reflects the contribution of the second-order mixing parameter to the reproduction of the lines at the peak.

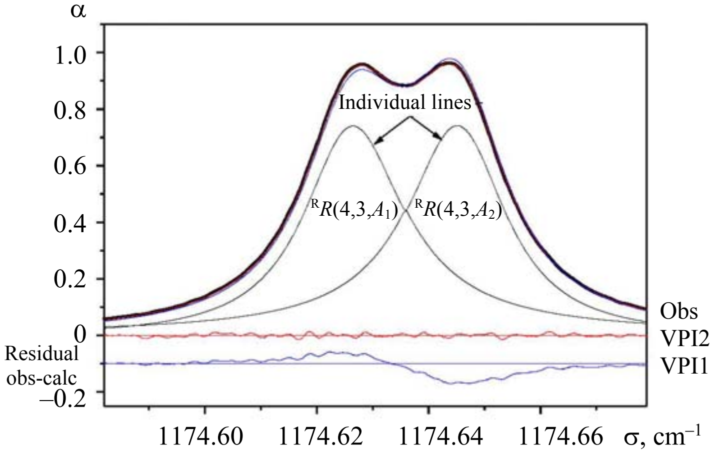

Fig. 2. The measured profile for the A_1A_2 components of the $^{R}R(4,3)$ doublet transition in the ν_4 band of PH_3 diluted by 100.77 mbars of H_2 (solid lines), and fitted superposed theoretical profiles VPI2 and VPI1. The deviations from the fit (obs-calc) residuals from VPI2 and VPI1. The (obs-calc) residuals are multiplied by 5 and displaced vertically for visibility.

Results and discussion. *Line intensities.* Using the absolute line intensities S_0 [18], the absorption path length l, and the constant partial pressure of PH_3 (P_{PH3}) in the gas mixtures, we have deduced the intensity parameter S for each studied transition. This parameter is fixed in the fit profiles used for all four recorded spectra broadened by four H_2 pressures. Consequently, we can fit the first- and second-order line mixing parameters PY and P^2g, respectively. This concept allows us to distinguish the proper line intensity from the rate of intensity transferred with the neighboring line during the overlap.

Figure 3 gives qualitative examples showing the difference between the intensity distribution in two overlapping lines obtained in this work, $S(1 + P^2g)$; the line intensities are presented with their errors ($S \pm \Delta S$) deduced from the results of [18]. These examples are presented for the A_1 and A_2 lines of the doublets $^{Q}R(8,3)$ in the ν_2 band and $^{R}R(4,3)$ in the ν_4 band of PH_3 vs. the square of the pressure of hydrogen P^2. We observe an almost linear variation of the intensity distribution between the two overlapping A_1 and A_2 lines vs P^2. The slopes of the straight lines of these variations have opposite signs. Table 2 shows that the variation of the intensity distribution obtained by this work sometimes exceeds the measurement uncertainties of the line intensities. They also differ from Brown's measurements [28], and they can reach 6.68% in the case of the line $^{Q}R(8,3,A_1)$.

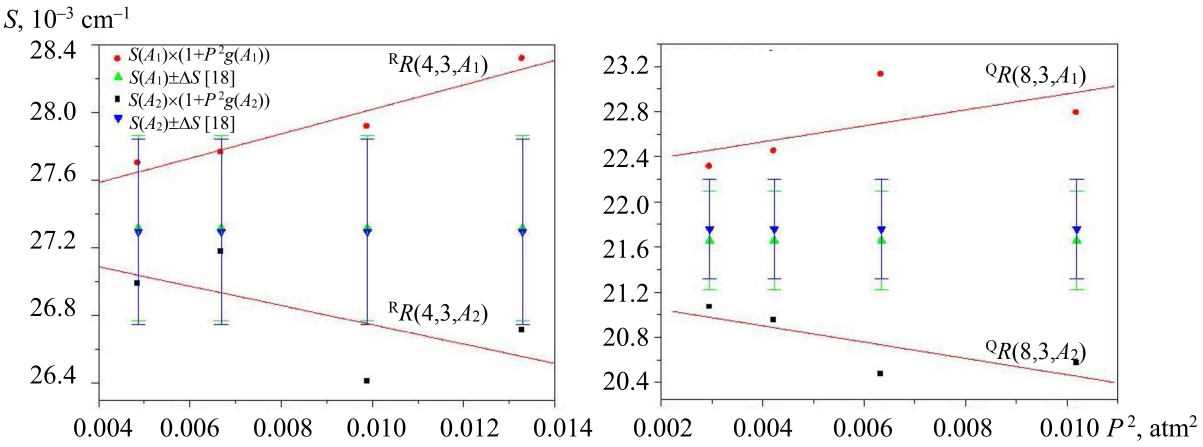

Fig. 3. Qualitative examples showing the difference between the intensity distribution in two overlapping lines: $S(1+P^2g)$ obtained in this work and the line intensities presented with their errors ($S\pm\Delta S$) deduced from the results [18]. These examples are presented for the A_1 and A_2 lines of the doublets $^{Q}R(8,3)$ in the ν_2 band and $^{R}R(4,3)$ in the ν_4 band of PH_3 vs. the square of the pressure of hydrogen P^2.

TABLE 2. Measured Line Intensities for the A_1A_2 Components of the Doublets Transition in the ν_2 and ν_4 Bands of PH_3 with their Estimated Errors

Transition	σ, cm^{-1} [23]	Line Intensity, 10^{-3} cm^{-1}			Diff, %
		($S\pm\Delta S$) [18]	S' [28]	$S(1+P^2g)$ this work	
ν_2 band					
$^{Q}R(8,3,A_1)$	1059.14042	21.656 ± 0.433	21.678	22.311→23.127	2.92–6.68
$^{Q}R(8,3,A_2)$	1059.14988	21.831 ± 0.438	21.590	21.064→20.471	2.43–5.18
$^{Q}R(9,3,A_1)$	1065.05928	16.570 ± 0.330	16.470	16.535→16.667	0.39–1.20
$^{Q}R(9,3,A_2)$	1065.07558	16.483 ± 0.330	16.470	16.488→16.280	0.11–1.15
ν_4 band					
$^{R}R(4,3,A_1)$	1174.62613	27.317 ± 0.548	27.317 [18]	27.700→28.319	1.40–3.67
$^{R}R(4,3,A_2)$	1174.64546	27.311 ± 0.548	27.363	27.175→26.407	0.69–3.49

Broadening coefficients and line mixing effects. Figure 4 shows a typical linear regression of the values of the collisional half-width measured at each of the four pressures of H_2 for the $^{R}R(4,3)$ doublet A_1 and A_2 lines of PH_3. The collisional half-widths are measured using the VPI2 profile. The slopes of the straight lines correspond to the H_2-broadening coefficients γ_0 (in 10^{-3} cm^{-1}atm^{-1}). Here, we have systematically considered the small self-broadening contributions (represented by a point close to the origin) derived from the self-broadening coefficients calculated using the theoretical model detailed [6] and from the constant partial pressure of PH_3 in the gas mixtures. The measurements of γ_0 was presented in Table 3 with their errors given by the standard deviation derived from the linear least-squares fit. The average values of the broadening coefficients of the A_1 and A_2 lines are in good agreement with those obtained in [18], where the second-order mixing parameter is neglected. However, any appreciable difference between the coefficients of each line is shown as a percentage in Table 3. This behavior reflects the line mixing effect on the line widths, and it is shown by considering the second-order mixing term given by Smith's development. In the same branch, the line mixing effect on the width decreases with the rotational quantum number J, i.e., when the difference wavenumber $\Delta\sigma$ increases (Table 3).

Line shifting parameters. Figure 5 depicts a typical plot of the line shift δ derived from the VPI2 profile versus the H_2 pressure P for the $^{R}R(4,3,A_1)$ and $^{R}R(4,3,A_2)$ lines in the ν_4 band of PH_3. The point close to the origin represents the self-shifting contribution (δ_{self}). The measured values show a quadratic dependence on pressure, which agrees with the theoretical analyses given by the development of Smith's second-order per-

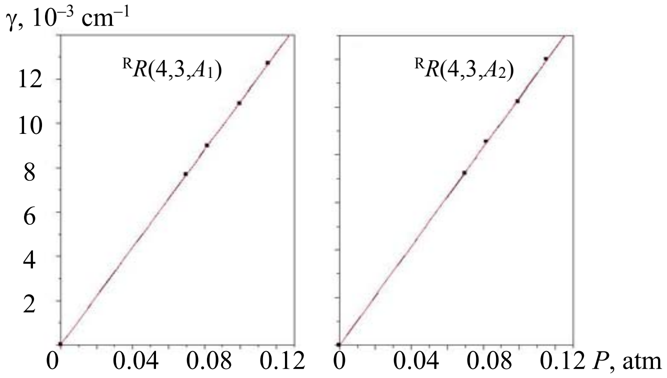

Fig. 4. The linear regression of the collisional width γ for the $^{R}R(4,3)$ doublet A_1 and A_2 lines in the ν_4 band of PH_3, derived from the fit of VPI2 (▪). The point close to the origin represents the self-broadening contribution.

TABLE 3. Measured H_2-Broadening Coefficients for the A_1A_2 Components of the Doublets Transition in the ν_2 and ν_4 Bands of PH_3 with Their Estimated Errors

Transition	σ, cm^{-1} [23]	$\Delta\sigma$, cm^{-1}	γ_0, 10^{-3} cm^{-1}atm^{-1}		$\Delta\gamma_0/\gamma_{0Av}$, %	[18]
			VPI2	γ_{0Av}		
			ν_2 band			
$^{Q}R(8,3,A_1)$	1059.14042	0.00946	102.27 (1.07)	100.5 (2.6)	3.48	98.01 (0.76)
$^{Q}R(8,3,A_2)$	1059.14988		98.77 (0.58)			97.25 (0.55)
$^{Q}R(9,3,A_1)$	1065.05928	0.01630	96.34 (1.13)	96.5 (1.1)	0.34	97.31 (0.16)
$^{Q}R(9,3,A_2)$	1065.07558		96.67 (0.71)			97.20 (0.53)
			ν_4 band			
$^{R}R(4,3,A_1)$	1174.62613	0.01933	109.97 (0.96)	106.8 (4.8)	5.85	107.15 (0.24)
$^{R}R(4,3,A_2)$	1174.64546		103.72 (2.31)			106.83 (0.50)

Note. $\Delta\sigma = |\sigma(A_1) - \sigma(A_2)|$, $\gamma_{0Av} = [\gamma_0(A_1) + \gamma_0(A_2)]/2$, $\Delta\gamma_0 = |\gamma_0(A_1) - \gamma_0(A_2)|$.

turbation theory [19]. Consequently, from the unconstrained second-order polynomial least-squares procedures, we deduce the first-and second-order coefficients of the curves, which are the first-order δ_0 and second-order $\delta\sigma$ H_2-shift coefficients, respectively. Indeed, the line-shift parameter for each line k is expressed in the framework of the development of the second-order perturbation theory as

$$\delta_k = \delta_{self} + P\delta_{0k} + P^2\delta\sigma_k, \tag{5}$$

where the first-order coefficient δ_{0k} is related to the imaginary part of the diagonal (W_{kk}) elements of the collisional relaxation matrix (W), and the second-order coefficient $\delta\sigma_k$ is related to their off-diagonal elements ($W_{kk'}$ with $k' \neq k$) by [19]:

$$\delta\sigma_k = \sum_{k' \neq k} \frac{W_{kk'}W_{k'k}}{\sigma_{0k'} - \sigma_{0k}}. \tag{6}$$

We only present the qualitative behavior of the line-shift parameter with the perturber pressure. This behavior agrees with the hypothesis of second-order Smith's development.

First-order line mixing parameter. Figure 6 depicts two examples of the variation of the fitted first-order line mixing parameter (PY) by VPI2, with H_2 pressure P for the A_1 and A_2 lines of the $^{R}R(4,3)$ doublet in the ν_4 band of PH_3. The first-order H_2-line mixing coefficients Y are deduced from the slope of the straight lines resulting from unconstrained linear least-squares procedures. These values obtained with their errors, given by the standard deviation on Y derived from the linear least-squares fit, are presented in Table 4.

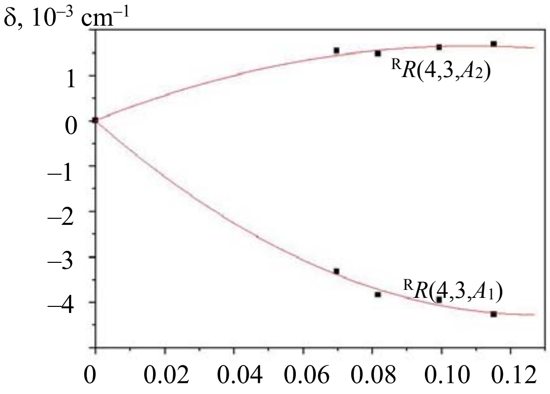

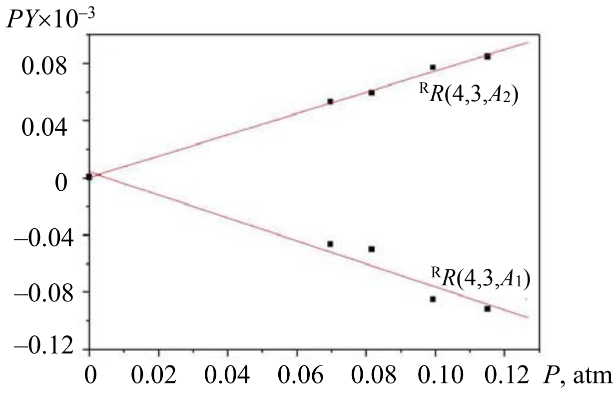

Fig. 5. The pressure dependence of the line shifts δ for the $^{R}R(4,3)$ doublet A_1 and A_2 lines in the ν_4 band of PH_3, derived from the fit of VPI2 (▪). The point close to the origin represents the self-shifting contribution. The best fit curves represent the second-order polynomial functions whose first- and second-order coefficients are, respectively, the first- and second-order H_2-shifting coefficients for each transition.

Fig. 6. The pressure dependence of the first-order mixing parameter PY for the A_1A_2 components of the $^{R}R(4,3)$ doublet transition in the ν_4 band of PH_3, derived from the fit of VPI2 (▪). The slopes of the best-fit lines represent the first-order H_2-line mixing coefficients for each transition.

TABLE 4. First and Second-Order H_2-Line Mixing Coefficients for the A_1A_2 Components of the Doublets Transition in the ν_2 and ν_4 Bands of PH_3 with Their Estimated Errors

Transition	σ, cm^{-1} [23]	$\Delta\delta$, cm^{-1}	Y, 10^{-3} atm^{-1}		g, 10^{-3} atm^{-2}
			VPI2	[18]*	VPI2
ν_2 band					
$^{Q}R(8,3,A_1)$	1059.14042	0.00946	–1.77 (0.16)	–3.23 (0.40)	3.28 (1.74)
$^{Q}R(8,3,A_2)$	1059.14988		1.71 (0.27)	3.31 (0.56)	–3.30 (1.05)
$^{Q}R(9,3,A_1)$	1065.05928	0.01630	–1.32 (0.04)	–1.47 (0.59)	0.93 (0.15)
$^{Q}R(9,3,A_2)$	1065.07558		0.92 (0.44)	0.86 (0.27)	–1.45 (0.30)
ν_4 band					
$^{R}R(4,3,A_1)$	1174.62613	0.01933	–1.12 (0.23)	–0.92 (0.22)	2.65 (0.27)
$^{R}R(4,3,A_2)$	1174.64546		0.74 (0.07)	0.76 (0.43)	–2.09 (0.95)

Note. $\Delta\sigma = |\sigma(A_1) - \sigma(A_2)|$.

* These values correspond to the average of the measurements obtained with the two models (VP with mixing and SDRP with mixing).

For the components A_1 and A_2 of the doublet lines, the first-order mixing coefficients are opposite. Except for the mixing coefficients of $^{Q}R(8,3)$ doublet lines, where it is underestimated, the results presented in this work satisfactorily agree with those given in [18]. In the ^{Q}R branch, the first-order mixing coefficients show a decrease in absolute value with the rotational quantum number J, that is, when the difference wavenumber $\Delta\sigma$ increases (Table 4). The line mixing (off-diagonal relaxation elements) coefficients (W_{ij}) for the A_1A_2 pairs of transitions in the phosphine pentad are given by V. Malathy Devi et al. [29] are seen and compared to ours.

Second-order line mixing parameter. Two typical examples of the variation of the second-order line mixing parameter (P^2g) deduced by fitting with the VPI2 profile vs. the square of the pressure of hydrogen P^2 are shown in Fig. 7 for the $^{R}R(4,3)$ doublet A_1 and A_2 lines in the ν_4 band of PH_3. The second-order H_2-line mixing coefficients g are derived from the slope of the straight lines resulting from unconstrained linear least-squares procedures. Presented in Table 4, these values are obtained with their errors, given by the standard deviation on g derived from the linear least-squares fit. The measurement uncertainties are less than 31.8% for the studied transitions, except for the $^{Q}R(8,3,A_1)$ and $^{R}R(4,3,A_2)$ lines, which are in the range of 53 and 45%, respectively. For each doublet line A_1 and A_2, these second-order mixing coefficients are the opposite, which reflects the rate of intensity exchange during the overlap due to the population transfer between low energy levels of the two transitions. With the pressure range considered in this work, the second-order mixing term becomes appreciable. Thereafter, it is measurable, while at lower pressures it is indistinguishable from the measured uncertainties of line intensities, such as the case of the spectra studied in [18]. Like the observed behavior of the first-order mixing parameter, the latter shows a decrease with the rotational quantum number J in the ν_2 band as the difference wavenumber $\Delta\sigma$ increases (Table 4).

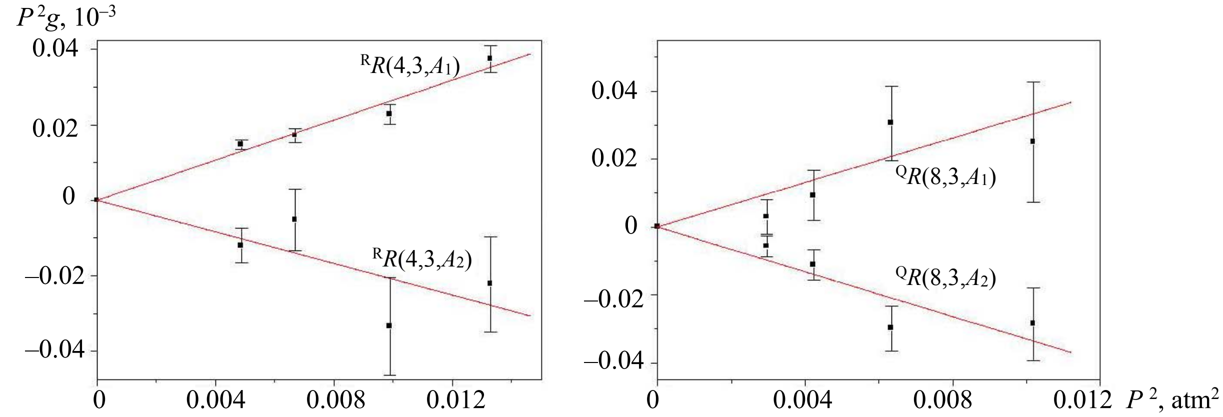

Fig. 7. Variation of the second-order mixing parameter P^2g with their bar error vs. the square of the H_2-pressure for the A_1A_2 components of the doublets transition $^{Q}R(8,3)$ in the ν_2 band and $^{R}R(4,3)$ in the ν_4 band of PH_3, derived from the fit of VPI2 (▪). The slopes of the best-fit lines represent the second-order H_2-line mixing coefficients for each transition.

Conclusions. This work presents reasonable first-and second-order mixing coefficients within the framework of the second-order approximation of perturbation theory for some lines in the ν_2 and ν_4 bands of PH_3 perturbed by H_2 at room temperature. To achieve these results, we used the spectra recorded at pressures ranging from 55 to 117 mbar using a diode laser spectrometer. We also have considered the collisional profile proposed by Smith [19] and developed within the framework of the second-order perturbation theory. This allows us to deduce the VPI2 profile by convolution with the Doppler profile.

The obtained shifting parameter shows a parabolic variation with the perturber pressure, which is justified by the second-order approximation used. We have set the intensity parameter in the fit profiles; this allows us to distinguish between the appropriate line intensity and the intensity rate exchanged with the neighboring line during the overlap. Consequently, we have shown that the second-order mixing parameter is appreciable and measurable. Indeed, it expresses the rate of intensity transferred between the overlapping lines A_1 and A_2 of each doublet. During this work, we have demonstrated the line mixing effect on the line widths, which allows us to better understand the collisional dynamics of the molecules.

Acknowledgments. The authors J. Salem and R. Charguia gratefully acknowledge financial support by Qassim University represented by the Deanship of Scientific Research through the Project Number 3619-cosabu-2018-1-14-S.

REFERENCES

1. S. T. Ridgway, L. Wallace, G. R. Smith, *Astrophys. J.*, **207**, 1002–1006 (1976).
2. R. A. Hanel, B. Conrath, M. Flasar, V. Kunde, P. Lowman, W. Maguire, J. Pearl, J. Pirraglia, *Science*, **204**, 972–976 (1979), doi: 10.1126/science.204.4396.972-a.
3. V. Kunde, R. Hanel, W. Maguire, D. Gautier, J. P. Baluteau, A. Marten, A. Chedin, N. Husson, N. Scott, *Astrophys. J.*, **263**, 443–467 (1982).
4. H. P. Larson, U. Fink, H. A. Smith, D. Scott Davies, *Astrophys. J.*, **240**, 327–337 (1980).
5. J. P. Bouanich, J. Salem, H. Aroui, J. Walrand, G. Blanquet, *J. Quant. Spectrosc. Radiat. Transf.*, **84**, 195–205 (2004), doi: 10.1016/S0022-4073(03)00143-2.

6. J. Salem, H. Aroui, J. P. Bouanich, J. Walrand, G. Blanquet, *J. Mol. Spectrosc.*, **225**, 174–181 (2004), doi: 10.1016/j.jms.2004.02.025.
7. J. Salem, J. P. Bouanich, J. Walrand, H. Aroui, G. Blanquet, *J. Mol. Spectrosc.*, **228**, 23–30 (2004), doi: 10.1016/j.jms.2004.06.015.
8. J. Salem, J. P. Bouanich, J. Walrand, H. Aroui, G. Blanquet, *J. Mol. Spectrosc.*, **232**, 247–254 (2005), doi: 10.1016/j.jms.2005.04.014.
9. J. P. Bouanich, J. Walrand, G. Blanquet, *J. Mol. Spectrosc.*, **232**, 40–46 (2005), doi: 10.1016/j.jms.2005.02.005.
10. J. P. Bouanich, G. Blanquet, *J. Mol. Spectrosc.*, **241**, 186–191 (2007), doi: 10.1016/j.jms.2006.12.006.
11. J. Salem, G. Blanquet, M. Lepère, H. Aroui, *J. Mol. Spectrosc.*, **297**, 58–61 (2014), doi: org/10.1016/j.jms.2014.01.003.
12. J. Salem, G. Blanquet, M. Lepère, H. Aroui, *J. Quant. Spectrosc. Radiat. Transf.*, **173**, 34–39 (2016), http://dx.doi.org/10.1016/j.jqsrt.2016.01.010.
13. G. Dufour, D. Hurtmans, A. Henry, A. Valentin, M. Lepère, *J. Mol. Spectrosc.*, **221**, 80–92 (2003), doi: 10.1016/S0022-2852(03)00178-4.
14. N. Maaroufi, F. Kwabia Tchana, X. Landsheere, H. Aroui, *J. Quant. Spectrosc. Radiat. Transf.*, **219**, 383–392 (2018), https://doi.org/10.1016/j.jqsrt.2018.09.001.
15. F. Hmida, S. Galalou, F. Kwabia Tchana, M. Rotger, H. Aroui, *J. Quant. Spectrosc. Radiat. Transf.*, **189**, 351–360 (2017), https://doi.org/10.1016/j.jqsrt.2016.12.015.
16. L. Fissiaux, G. Blanquet, M. Lepère, *J. Quant. Spectrosc. Radiat. Transf.*, **113**, 1233–1239 (2012), doi: 10.1016/j.jqsrt.2012.01.021.
17. F. Thibault, J. Boissoles, R. Le Doucen, R. Farrenq, M. Morillon-Chapey, C. Boulet, *J. Chem. Phys.*, **97**, 4623–4632 (1992), doi: 10.1063/1.463865.
18. J. Salem, G. Blanquet, M. Lepère, R. ben Younes, *Mol. Phys.*, **116**, 1280–1289 (2018), doi: 10.1080/00268976.2017.1423125.
19. E. W. Smith, *J. Chem. Phys.*, **74**, 6658–6673 (1981), http://dx.doi.org/10.1063/1.441112.
20. P. W. Rosenkranz, *IEEE. Trans. Antenn. Propag.*, **23**, 498–506 (1975), doi: 10.1109/TAP.1975.1141119.
21. E. Baeten, G. Blanquet, J. Walrand, C. P. Courtoy, *Can. J. Phys.*, **62**, 1286–1292 (1984), doi: 10.1139/p84-174.
22. M. Lepère, G. Blanquet, J. Walrand, J. P. Bouanich, *J. Mol. Spectrosc.*, **180** 218–226 (1996), https://doi.org/10.1006/jmsp.1996.0245.
23. W. H. Press, B. P. Flannery, S. A. Tendolsky, W. T. Vetterling, Numerical Recipes – The Art of Scientific Computing (FORTRAN Version), Cambridge Univ. Press, Cambridge (1992).
24. Hitran Data Bases, http://www.hitran.org/results/5a1856e6.par.
25. G. Blanquet, J. Walrand, J. P. Bouanich, *J. Mol. Spectrosc.*, **159**, 137–143 (1993), https://doi.org/10.1006/jmsp.1993.1112.
26. J. Humlíček, *J. Quant. Spectrosc. Radiat. Transf.*, **21**, 309–313 (1979), https://doi.org/10.1016/0022-4073(79)90062-1.
27. A. S. Pine, *J. Quant. Spectrosc. Radiat. Transf.*, **57**, 145–155 (1997), https://doi.org/10.1016/S0022-4073(96)00129-X.
28. L. R. Brown, R. L. Sams, I. Kleiner, C. Cottaz, L. Sagui, *J. Mol. Spectrosc.*, **215**, 178–203 (2002), doi: 10.1016/S0022-2852(02)98638-8.
29. V. M. Devi, D. C. Benner, I. Kleiner, R. L. Sams, L. N. Fletcher, *J. Mol. Spectrosc.*, **302**, 17–33 (2014), https://doi.org/10.1016/j.jms.2014.06.003.